Chapter 6

Production and recycling of oceanic crust in the early Earth

Abstract

Because of the strongly different conditions in the mantle of the early Earth regarding temperature and viscosity, present-day geodynamics cannot simply be extrapolated back to the early history of the Earth. We use numerical thermochemical convection models including partial melting and a simple mechanism for melt segregation and oceanic crust production to investigate an alternative suite of dynamics which may have been in operation in the early Earth. Our modelling results show three processes that may have played an important role in the production and recycling of oceanic crust: (1) Small scale ($x \cdot 100km$) convection involving the lower crust and shallow upper mantle. Partial melting and thus crustal production takes place in the upwelling limb and delamination of the eclogitic lower crust in the downwelling limb. (2) Large scale resurfacing events in which (nearly) the complete crust sinks into the (eventually lower) mantle, thereby forming a stable reservoir enriched in incompatible elements in the deep mantle. New crust is simultaneously formed at the surface from segregating melt. (3) Intrusion of lower mantle diapirs with a high excess temperature (about 250 K) into the upper mantle, causing massive melting and crustal growth. This allows for plumes in the Archean upper mantle with a much higher excess temperature than previously expected from theoretical considerations.

6.1 Introduction

As no oceanic crust on Earth is older than about 200 million years, we have no direct evidence on the nature of oceanic crust in the early Earth. Obducted oceanic sequences in

This chapter has been submitted by P. van Thienen, A.P. van den Berg and N.J. Vlaar for publication in *Tectonophysics*.

the form of ophiolites, in a strict definition, go back to about 800-900 million years before present, or back to about 2000 Ma when a broader definition is applied (Helmstaedt and Scott, 1992). The Archean, however, lacks ophiolites (Hamilton, 1998). A recent find of a 2.505 Ga ophiolite sequence in North China (Kusky et al., 2001) has been disputed by others (Zhai et al., 2002).

From theoretical considerations, several characteristics can be inferred about oceanic lithosphere in the early Earth. As a consequence of the higher mantle temperature, partial melting in shallow convective upwellings produced a layering of basaltic crust and underlying depleted (lherzolitic-harzburgitic) mantle peridotite much thicker than expected under modern day mid-oceanic ridges. As the extent of the continents is thought to have progressively grown through the Earth's history (McCulloch and Bennett, 1994), the extent of the complementary part that is the oceanic domain must have been larger than it is today. The more extensive differentiation of mantle peridotite generates more positive chemical buoyancy which takes a much longer time to be balanced by negative buoyancy due to cooling, and which would therefore be much more difficult to subduct on reasonable time scales (Sleep and Windley, 1982; Vlaar, 1985, 1986; Vlaar and Van den Berg, 1991). The dynamics of an oceanic lithosphere in the early Earth must therefore have been different from those in the present-day Earth. Crustal recycling must however have taken place because of the present relative paucity of Archean crustal material. Furthermore, isotopic evidence indicates crustal recycling during the Archean (Nielsen et al., 2002).

An alternative mechanism of recycling of oceanic crust into the mantle was proposed by Vlaar et al. (1994). When a basaltic crustal layer becomes sufficiently thick, a phase transition to eclogite may occur in the deeper parts (e.g. Hacker, 1996). In the presence of a sufficiently weak rheology, delamination of this dense crustal layer may take place and thus recycling of dense eclogite into the upper mantle. The space vacated by the delaminating eclogite can be filled up by inflowing mantle material, which may be fertile and undergo decompression melting, thus adding new material to the crust. This recycling mechanism may have contributed significantly to the early cooling of the Earth during the Archean (Vlaar et al., 1994). However, as the fertile mantle material replacing delaminated eclogite only undergoes partial melting, it produces a smaller volume of crust compared to the crust involved in the delamination. Therefore, the mechanism cannot be self-sustaining, since there is no complete recovery of the crust. An additional source of crustal material in the form of an active upwelling of fertile mantle rock (for example in mantle diapirs) is required to keep this process going. Related models concerning the delamination of eclogite have been presented by Parmentier and Hess (1992) in a general and abstract sense for terrestrial planets and by Zegers and Van Keken (2001) for the more specific subject of generation of continental material.

Geochemistry may give insight into the chemical state of the early Earth. Differentiation may be expected both in a solidifying magma ocean and during partial melting of an already solidified mantle.

The chemistry of the earliest material found on the present-day Earth's surface, 4.0-4.4 Ga detrital zircons (Wilde et al., 2001; Peck et al., 2001), indicates growth in a granitic magma, which means that production of continental crustal material and thus differentiation was already taking place.

The earliest continental rocks found on Earth (less than 4 Ga) show evidence in the form of isotope ratios (^{143}Nd/^{144}Nd, ^{176}Hf/^{177}Hf) that these rocks have been derived from a mantle source that was already depleted in incompatible elements (Hamilton et al., 1983; Patchett, 1983; Vervoort et al., 1996; Blichert-Toft et al., 1999). Amelin et al. (2000) give a minimum age estimate of the derivation of the depleted mantle from a uniform chondritic reservoir of 4.08 Ga, based on ^{176}Lu/^{177}Hf data. They also note an increasing trend with decreasing age in the degree of depletion of the mantle from which the crustal rocks they have investigated are indirectly derived (higher ϵ_{Hf} for the 3.45 Ga Barberton and Pilbara rocks than for the 3.68-3.73 Ga Amîtsoq gneisses).

Differentiation of the proto-mantle in a partially molten regime may be expected, but the result is only a change in the relative proportions of compatible and incompatible elements, retaining more or less chondritic relative abundances for the major elements (Abe, 1993b). Computations by Abe (1997) show that differentiation in a terrestrial magma ocean spanning at least the upper mantle probably took place and may be related to the Nd and Hf isotopic evidence for early mantle depletion.

On the basis of calculations of fractionation upon solidification of a terrestrial magma ocean of lithophile element ratios (Al/Ti, Ca/Ti, Ca/Al, Mg/Si, Si/Al) and comparison to primitive mantle ratios, McFarlane et al. (1994) conclude that ”there is no surviving evidence of mineral fractionation” (p. 5161), which in their opinion means that: (1) no significant magma ocean was ever present in the Earth, (2) vigorous convection suppressed segregation of minerals from the magma or (3) that mantle convection wiped out the evidence for fractionation afterwards. Presnall et al. (1998), however, consider this to be too poorly constrained by element partitioning data.

These combined results from geochemistry suggest that chemical differentiation in the early mantle was an important process, as seen from isotope ratios, but that large scale inhomogeneities may have been rapidly remixed, as suggested by lithophile element ratios. This makes it difficult to come up with a viable starting scenario for numerical models of the mantle in the early Earth.

Numerical mantle convection models starting from a pristine mantle show the development of chemical heterogeneity in the mantle. Depending on the rate of internal heating due to the decay of radioactive isotopes, stratification of depleted and undepleted mantle material or mixing of these may occur on whole mantle scale (Ogawa, 1988; Kameyama et al., 1996; Ogawa, 2000). Walzer and Hendel (1997) modeled a simplified chemical segregation in the mantle, generating continents. In a more complex setup, they modeled the development of distinct pristine lower mantle and depleted upper and uppermost lower mantle reservoirs (Walzer and Hendel, 1999). The development of chemical stratification in the upper mantle underneath continents was demonstrated in thermochemical convection models (De Smet et al., 1998; De Smet, 1999; De Smet et al., 2000a). In these models, a continental root of depleted peridotite of about 200 kilometers develops, underneath which the remaining part of the upper mantle remains relatively fertile. Similar models by Schott et al. (2001) applied to Mars produce a thick (500 km) buoyant layer of melt residue, inhibiting recycling of crustal material.

Here we present results of numerical modelling experiments of mantle convection including pressure release partial melting. The model includes a simple approximate melt

segregation mechanism and basalt to eclogite phase transition, to account for the dynamic accumulation and recycling of the crust in an upper mantle subject to secular cooling. The focus of our investigations is on the dynamics of the production of oceanic crust and its recycling through the eclogite phase into the mantle. We investigate the conditions that favor such a mechanism, and discuss its consequences for the cooling history of the Earth. We also investigate the development and sustainability of the chemical differentiation that is caused by the process, both concerning the major elements and incompatible trace elements.

6.2 Numerical model setup

6.2.1 Description of the numerical model

We have used a 2-D Cartesian thermo-chemical convection code including partial melting. An extended Boussinesq approach was used, assuming infinite Prandtl number, including viscous dissipation, adiabatic compression, and latent heat of melting. Partial melting is modeled as an (irreversible) increase in the *degree of depletion F*, which has been defined here as the mass fraction of melt that is extracted from an initially unmelted material control volume of mantle material. The melt that is produced is extracted instantaneously and deposited at the top boundary. Here the melt flux is transformed into an inflow boundary condition, thus producing a basaltic crust. In the current approximation, the compaction of the residual mantle due to this melt removal is neglected. Time dependent internal heating due to the decay of radioactive elements was included and coupled to the concentration of a single incompatible element, which has an initial concentration of 1 and fractionates upon partial melting with a distribution coefficient of 0.01 (see section 6.2.3). Undepleted mantle material is characterized by a time dependent heat productivity with an initial value of $15 \cdot 10^{-12} W kg^{-1}$ and a half life value of radioactive decay of 2.5 Ga. For the compositionally evolving mantle material this time dependent value is multiplied with the local trace element concentration. The extraction of heat producing elements during partial melting results in a concentration of the heat productivity in the basalt produced by the partial melting.

The model is described by the following non-dimensional equations (De Smet et al., 1998). The energy equation (see Table 6.1 for explanation of the symbols used):

$$\frac{dT}{dt} - Di(T+T_0)w = \nabla^2 T - \frac{\Delta S}{c_p}\frac{dF}{dt}(T+T_0) + \sum_k \gamma_k \frac{Rc_k}{Ra} Di(T+T_0)\frac{d\Gamma_k}{dt}$$

$$+\frac{Di}{Ra}\Phi + R_H H \tag{6.1}$$

The heating due to viscous dissipation is set to zero in the calculations to avoid extreme heating rates in the upper crust, where laterally varying amounts of crustal material is forced into the system at considerable rates, see below. We have verified that this has a minor effect on the resulting dynamics and thermal development of the subcrustal domain.

symbol	property	definition	value/unit
B_1	diffusion creep prefactor		Pas
B_2	dislocation creep prefactor		$\mathrm{Pa}^{\mathrm{n}_2}\mathrm{s}$
C_0	cohesion factor		0 Pa
c_p	heat capacity at constant pressure		$1250\ \mathrm{Jkg}^{-1}\mathrm{K}^{-1}$
E_1	diffusion creep activation energy		$270 \cdot 10^3 \mathrm{Jmol}^{-1}$
E_2	dislocation creep activation energy		$485 \cdot 10^3 \mathrm{Jmol}^{-1}$
e_{ij}	strainrate tensor	$\partial_j u_i + \partial_i u_j$	s^{-1}
e	second invariant of the strainrate tensor	$[\frac{1}{2} e_{ij} e_{ij}]^{\frac{1}{2}}$	s^{-1}
$f(F)$	composition dependent viscosity prefactor		
F	degree of depletion		
g	gravitational acceleration		$9.8\ \mathrm{ms}^{-2}$
h	length scale		$1005 \cdot 10^3$ m
H	radiogenic heat production		Wm^{-3}
n_1	diffusion creep stress exponent		1
n_2	dislocation creep stress exponent		3.25
n_y	yield exponent		10
P	pressure		Pa
R	Gas constant		$8.341 \mathrm{Jmol}^{-1}\mathrm{K}^{-1}$
Ra	thermal Rayleigh number	$\frac{\rho_0 \alpha \Delta T g h^3}{\kappa \eta_0}$	
Rb	compositional Rayleigh number	$\frac{\delta \rho g h^3}{\kappa \eta_0}$	
Rc	phase Rayleigh number	$\frac{\delta \rho g h^3}{\kappa \eta_0}$	
S	melt productivity function		s^{-1}
ΔS	entropy change upon full differentiation		$300\ \mathrm{Jkg}^{-1}\mathrm{K}^{-1}$
t	time		s
T	temperature		$^o\mathrm{C}$
T_0	non-dimensional surface temperature		$\frac{273}{\Delta T}$
ΔT	temperature scale		$2450\ ^o\mathrm{C}$
V_1	diffusion creep activation volume		$6 \cdot 10^{-6} \mathrm{m}^3\mathrm{mol}^{-1}$
V_2	dislocation creep activation volume		$17.5 \cdot 10^{-6} \mathrm{m}^3\mathrm{mol}^{-1}$
w	vertical velocity		ms^{-1}
z	depth		m
$\hat{z}$	unit vector in vertical (downward) direction		
$z_0(T)$	temperature dependent depth of phase transition		m
α	thermal expansion coefficient		$3 \cdot 10^{-5}\ \mathrm{K}^{-1}$
Γ	phase function	$\frac{1}{2}\left(1 + \sin(\pi \frac{z - z_0(T)}{\delta z})\right)$	
$\delta\rho$	density difference (chemical or phase)		kgm^{-3}
$\dot{\varepsilon}$	strainrate		s^{-1}
$\dot{\varepsilon}_y$	yield strainrate		$10^{-15}\mathrm{s}^{-1}$
η	viscosity		Pas
η_y	yield viscosity		Pas
κ	thermal diffusivity		$10^{-6}\ \mathrm{m}^2\mathrm{s}^{-1}$
μ	friction coefficient		0.03
ρ_0	reference density		$3416\ \mathrm{kgm}^{-3}$
σ_n	normal stress		Pa
τ_y	yield stress		Pa

Table 6.1: Symbols of the energy and momentum equations (equations (6.1), (6.2), (6.3)) and the depletion evolution equation (6.4).

We use the Stokes equation in combination with a continuity equation for an infinite Prandtl number incompressible fluid:

$$\nabla[\eta(\nabla\vec{u} + \nabla\vec{u}^T)] - \nabla\Delta p = (RaT + RbF - \sum_k Rc_k\Gamma_k)\hat{z} \tag{6.2}$$

$$\nabla \cdot \vec{u} = 0 \tag{6.3}$$

Evolution of the degree of depletion is described by the following equation:

$$\frac{dF}{dt} = S(p, T, F) \tag{6.4}$$

The source function S in (6.4) describes the distribution of partial melting, applying a simple parameterization of the melting phase diagram of mantle peridotite (De Smet et al., 1998). We use a third order polynomial parameterizations of the solidus and the liquidus, based on Herzberg and Zhang (1996), down to a depth of 400 km, assuming that melt produced below this depth is not segregated. Our isobaric melting curve, which is based on data presented by Jaques and Green (1980), is linear (see De Smet et al., 1998).

The set of equations (6.1)-(6.4) was solved using finite element methods and a Predictor-Corrector time integration scheme, described in Van den Berg et al. (1993). The different finite element meshes used contain approximately 2200 and approximately 5100 triangular elements respectively (see Table 6.2), with a nodal point spacing of approximately 10-15 km. Tests have shown this to be sufficient to resolve the dynamics, since at lower resolution some characteristics of the dynamics are lost whereas a higher resolution results in the same behavior. The field description of the degree of depletion field F was transported using a Lagrangian particle tracer method (300 000 to 400 000 tracers). Fourth order Runge-Kutta time integration is used to advect the particle tracers with the mantle flow velocity. The transformation of particle tracer field values (the degree of depletion) to finite element Gauss points uses a Particle in Cell algorithm (Hockney and Eastwood, 1988).

The density of mantle material is related to the degree of depletion F (Jordan, 1979; Vlaar and Van den Berg, 1991). Also, basalt has its own density and is transformed into heavier eclogite upon reaching depths in excess of 30 km in our model. The kinetics of this transition are approximated assuming a constant relaxation time for the transition of 1.25 Myr. The depth of 30 km (0.9 GPa) we use is somewhat less than the depth of about 40 km (1.2 GPa) that Hacker (1996) states as the minimum pressure of basalt to eclogite transformation. However, as we are dealing with melt products in a mantle that is hotter than the present, their composition is more MgO-rich than present day mid ocean ridge basalt (Nisbet, 1982). Experiments of Green and Ringwood (1967) have shown that the transition may occur at lower pressures and higher temperatures in MgO-rich rocks. Furthermore, lower pressure phase assemblages (above 0.7-0.8 GPa) may also contain garnet (Green and Ringwood, 1967; Ito and Kennedy, 1971; Hacker, 1996), thus raising the bulk density above that of the original basaltic phase assemblage. We do not consider phase boundary topography due to temperature effects, since we expect this to

model	initial conditions		domain		
	T_{pot}^{start} (C)	d_{crust}^{start} (km)	# elements	# boundary points	width & depth (km)
M0	1464	0.0	2245	67	1005
M0b	1464	0.0	2245	67	1200
M1	1896	20.1	2245	67	1005
M2	1948	25.6	2245	67	1005
M3	1976	30.0	2245	67	1005
M4	2000	35.4	2245	67	1005
M5	2017	39.8	2245	67	1005
M6	2051	50.5	2245	67	1005
Mr	1976	30.0	5101	100	1005
Ms	1976	29.7	5101	100	1200

Table 6.2: Characteristics of the different model experiments. Models M0 and M0b are startup runs with increased radiogenic heating (see text). T_{pot}^{start} is the potential temperature and d_{crust}^{start} is the average crustal thickness, both at the start of the experiment. The number of boundary points indicates the number of model points of the triangular elements used in the discretization of the domain on a single domain boundary and is included as a measure of 1-D resolution.

be dominated by kinetic effects because of the relatively low Clapeyron slope of about 1 MPa/K (Philpotts, 1990).

The phase transitions around 400 and 670 km depth are also taken into account separately for peridotite and eclogite, though without kinetics (i.e., it is assumed to occur instantaneous). The relevant parameters for these phase transitions are given in Table 6.3. The phase transition of eclogite into perovskitite lithology in the shallow lower mantle (e.g. Ringwood and Irifune, 1988; Irifune and Ringwood, 1993; Hirose et al., 1999) is not taken into account. Dynamic effects have been predicted of the density inversion between eclogite and postspinel peridotite in the uppermost lower mantle (Irifune and Ringwood, 1993) caused by the deeper position of the transition of eclogite relative to the postspinel transition of peridotite. As recent work has indicated that the transition takes place around 720 km depth (Hirose et al., 1999) rather than around 800 km (e.g. Irifune and Ringwood, 1993), and has a positive Clapeyron slope that would lift the phase transition to even shallower levels in a cool sinking eclogite body, Hirose et al. (1999) predict that 'basaltic crust with perovskitite lithology would gravitationally sink into the deeper mantle'(their p.53). Earlier numerical experiments of Christensen (1988) show that an eclogite layer trapped in this density inversion zone in the uppermost lower mantle would probably not survive in a convecting mantle. Recent experiments by Kubo et al. (2002), however, indicate that slow kinetics of the lower mantle phase transition of basaltic material may delay the transition on the order of 10 million years, which may increase the residence time and depth extent of the shallow lower mantle density inversion zone. We have validated our assumption of the minor importance of the shallow lower mantle eclogite density inversion by performing an experiment in which it is included (eclogite $430 kgm^{-3}$ lighter

transition	material	P_0 (GPa)	T_0 (K)	γ (Pa/K)	δz (km)	$\frac{\delta\rho}{\rho_0}$
400	peridotite	13.4	1756	$3 \cdot 10^6$	50	0.05
400	basalt	12.5	1747	$3 \cdot 10^6$	150	0.10
670	peridotite	22.4	1854	$-2.5 \cdot 10^6$	50	0.05

Table 6.3: Parameters of the phase transitions used in the models. The first column indicates the approximate depth of the transition, the column marked δz indicates the depth range over which the transition is smeared out and the last column gives the relative density contrast of the phase transition.

than peridotite between 670 and 720 km depth), which showed no significant stagnation of basaltic material in this density inversion zone. The density effects of the varying composition and phase transitions are accounted for in buoyancy contribution terms, scaled by the Rayleigh numbers Rb and Rc_k, in the momentum equation (6.2) (see also De Smet et al., 1998, 2000a).

6.2.2 Rheology

The deformation of material is accounted for by three separate deformation mechanisms, which are diffusion creep, dislocation creep, and brittle failure. The former two are described by the following equation:

$$\eta_i = f(F) B_i \exp\left[\frac{E_i + PV_i}{RT}\right] \sigma^{1-n_i} \tag{6.5}$$

which is the standard Arrhenius formulation (Karato and Wu, 1993; Van den Berg and Yuen, 1998) with the addition of a composition dependent prefactor $f(F)$. The index i indicates the mechanism, either 1 for diffusion creep or 2 for dislocation creep. The other symbols are explained in Table 6.1. The activation energies E_i and volume V_i are based on Karato and Wu (1993), as is the prefactor, in which an assumed constant and uniform grain size of 1 mm is incorporated. The composition dependent prefactor $f(F)$ has a value of 1 for fertile peridotite and basalt (which have the same viscosity parameters in our models). For depleted peridotite (harzburgite) we apply a prefactor value of 10 for a degree of depletion over 0.05, and a linearly increasing value between $F = 0.005$ and $F = 0.05$ from 1 to 10 (Van Thienen et al., 2003a, chapter 8). This is intended to mimic the effect of dehydration during partial melting on the viscosity (Karato, 1986; Hirth and Kohlstedt, 1996; Mei and Kohlstedt, 2000a,b).

For eclogite, the viscosity prefactor $f(F)$ has a value of 0.1. Although Jin et al. (2001) find that for an eclogite with equal amounts of the two main constituents garnet and omphacite, the strength is comparable to harzburgite (which is hydrous in their experiments), Piepenbreier and Stöckhert (2001) find evidence in eclogite microstructures for a much lower flow strength than predicted from omphacite experimental flow laws. We translate this result to our latter viscosity prefactor value of 0.1.

The third deformation mechanism, brittle failure, is approximated by a yield mechanism which is included to reproduce fracturing-like behavior when the stress supersedes a certain yield stress τ_y. We use the formulation of Van Hunen et al. (2002):

$$\eta_y = \tau_y \dot{\varepsilon}_y^{-1/n_y} \dot{\varepsilon}^{(1/n_y)-1} \tag{6.6}$$

The symbols are explained in Table 6.1. We prescribe the yield stress τ_y, the yield strain rate $\dot{\varepsilon}_y$ and the yield exponent n_y. The latter describes the brittleness of the behavior (Van Hunen et al., 2002). We apply a value of 10, which gives a reasonable approximation of pure brittle behavior. The yield strength τ_y is determined as a function of depth using Byerlee's law (e.g. Lockner, 1995):

$$\tau_y = C_0 + \mu\sigma_n \tag{6.7}$$

in which we approximate the normal stress with the lithostatic pressure (e.g. Moresi and Solomatov, 1998):

$$\tau_y = C_0 + \mu\rho g z \tag{6.8}$$

We use a low value of 0.03 for the friction coefficient μ, consistent with results of Moresi and Solomatov (1998) for the mobilization of the Earth's lithosphere, and assume the cohesion term C_0 to be of minor importance and set it to 0.

The diffusion and dislocation creep viscosities are inversely added to define an effective ductile creep viscosity (Van den Berg et al., 1993) and the minimum of this value and the local yield viscosity is used for the local effective viscosity.

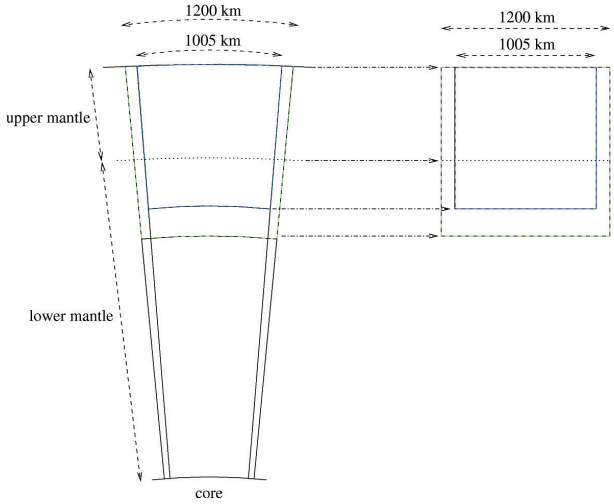

Figure 6.1: Setup of the 2-D square model domain measuring 1005 x 1005 km and 1200 x 1200 km in respective models listed in Table 6.2, representing the upper mantle and part of the lower mantle.

6.2.3 Fractionation of trace elements

The behavior of a single incompatible trace element is monitored in the models using the particle tracers. Upon partial melting, the concentration of the trace element is adjusted in each tracer using an equilibrium melting formulation (see e.g. Philpotts, 1990) for each integration time step (which essentially means that we assume equilibration between the melt and the residue during an integration time step, and consider a new batch of melt in the following time step). As mentioned above, the internal heating rate is a function of trace element concentration in the models. The result is that an enriched crust (generally by a factor 5-20) and a depleted residual mantle are formed.

The most important heat producing species in the Archean mantle are U and Th. These have bulk partition coefficients of $1.1 \cdot 10^{-4}$ and $1.7 \cdot 10^{-4}$, respectively, for spinel peridotites in equilibrium with a basaltic melt (Beattie, 1993), though temperature, composition, oxygen fugacity and the presence of volatiles may influence these values. We prescribe a distribution coefficient of 10^{-2} for the single incompatible heat producing element in our model which represents both U and Th. The value of the partition coefficient is somewhat larger than the values mentioned above for spinel peridotites. It is however small enough to allow significant fractionation and thus redistribution of heat productivity, but not so small that different degrees of melting result in the same residue concentrations of virtually zero. This allows us to regard the development of our trace element in a more general sense rather than limited to U and Th.

6.2.4 Model geometry and boundary conditions

For most models, we use a square computational domain of 1005 by 1005 km (see Figure 6.1), resulting in an upper mantle aspect ratio of 1.5. One extended model has dimensions of 1200x1200 km, resulting in an upper mantle aspect ratio of 1.8 (see section 6.3.4). We use a prescribed velocity on the upper boundary (controlled by basalt generation), periodical side boundaries and free slip conditions on the lower boundary. On the upper boundary we prescribe a temperature of 0^oC. Although we are dealing with the early Earth, the presence of liquid water on the surface, as indicated by oxygen isotope ratios in zircons of up to 4.4 Gyr old (Wilde et al., 2001; Peck et al., 2001), validates this assumption. On the lower boundary we prescribe a zero heat flux boundary condition to approximate conditions of transient secular cooling of the model by excluding heat input from below.

6.3 Results

As the initial condition for the models (i.e. the state of the Earth after solidification of the magma ocean) is difficult to reconstruct, we start from a model configuration including an initial basaltic crust and underlying depleted zone. We first test the sensitivity of the long-term development of the models to the initial situation (temperature and initial thickness of crust and depleted zone). The results will be presented in section 6.3.1. After this,

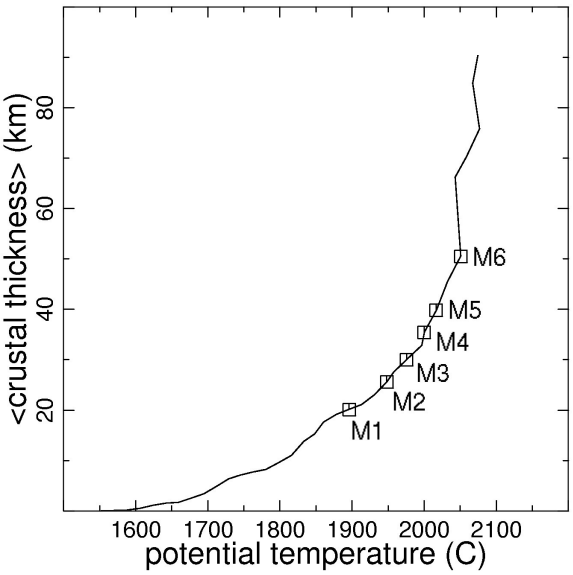

Figure 6.2: Development of the potential temperature and average crustal thickness of the initial model M0. Time progresses from the lower left to the upper right part of the curve. Symbols indicate the snapshots that are used as starting points for different cooling models (see Table 6.2).

the dynamics of crustal growth and recycling will be shown from the results of the model calculations (section 6.3.2). Next, we will present the long-term development of a number of models in section 6.3.3, and finally, the effect of the size of the model lower mantle is considered in section 6.3.4.

6.3.1 Sensitivity to initial conditions

We generate initial situations including a basaltic crust by starting model M0 (and M0b for a model with a larger domain width, see Table 6.2) with a uniform fertile composition, a geotherm that is below the solidus in the entire domain and a strongly increased internal heating of $250 \cdot 10^{-12}$ W/kg. The model rapidly heats up and starts melting, thus producing a crust. Different snapshots from the development of model M0 are used as starting points for a number of cooling and recycling models (M1-M6 in Table 6.2). Figure 6.2 shows the development of the potential temperature and accumulated crustal thickness for the startup model M0. The symbols in Figure 6.2 indicate the snapshots from which the cooling and recycling models are started. These are listed, together with their characteristics, in Table 6.2. In the cooling and recycling models M1-M6, the clock is initially reset to t=0, the internal heating is reset to $15 \cdot 10^{-12}$ W/kg (fertile mantle material value

representative of the early Earth), and natural decay with a half life of 2.5 Gyr is included.

In the two models with the thickest crust and highest initial temperature (M5 and M6, see Table 6.2), the entire crust sinks into the mantle within the first few million years of the model evolution. This is a result of the fact that a large part of the crust is transformed into the dense eclogite phase. The upwelling hot mantle material that replaces it locally completely melts, bringing the system back into a magma ocean regime. As our model assumptions are only valid for modest degrees of melting, we do not continue the calculations at complete melting, which is observed here. The results do show that a very thick basaltic crust of 40 km or more thickness is not sustainable on top of a hot, weak mantle in the early Earth.

The four somewhat cooler models M1-M4 (see Table 6.2) show higher rates of activity (vigor of convection and melt productivity) for higher initial temperature and greater crustal thickness. As a result of the higher crustal production rate, a higher cooling rate is observed for the hotter models, so that their volume averaged temperatures and surface heat fluxes converge after some hundreds of millions of years.

6.3.2 Dynamics of crustal growth and recycling

Three distinctive types of dynamics can be discerned in the process of crustal growth and recycling. The first is a small scale circulation near the bottom of the crust that transports eclogite down into the mantle and which produces new crust by partial melting of the upwelling part of the circulation. Figure 6.3 shows the development of such a coupled system in a zoom-in of model Mr. The left-hand frames show the composition field (individual particle tracers are plotted for basalt (black) and eclogite (red)), and the right-hand frames the temperature field (colors) and circular to oblong melt production zones (blue contours). In Figure 6.3a, no eclogite delamination is taking place but partial melting occurs in the upwelling flow near the right hand side thickened crustal region as indicated by the melting contours in the temperature frame. The melt that is produced is instantaneously transported vertically to the surface where it adds new material to the locally thickened crust. In the next frame (Figure 6.3b), eclogite starts to move downwards. At the same time, we see a similar but mirrored circulation arising below the left hand side thickened crustal region. About 4 million years later (Figure 6.3c), active delamination can be observed in both circulation systems, with high velocities in the common downwelling limb of the shallow circulations. Partial melting continues in the upwelling parts as indicated by the blue contours in the corresponding temperature snapshot. The recycling of eclogite into the mantle continues for tens of millions of years (see Figure 6.3d, 29 million years later).

Larger scale upwellings may add significantly more material to the crust. Figure 6.4 illustrates the development of a diapir originating from a lower mantle upwelling. As in Figure 6.3, the left-hand frames show the composition field and the right-hand frames the temperature field and the melting zone, which is quite large in this case. Because of its lower mantle origin, the material is both hot and fertile, indicated by the deep blue color, and starts melting at 400 km depth (which is the imposed maximum depth of melting in the model) in Figure 6.4a. Melting continues up to about 150 km depth, where the

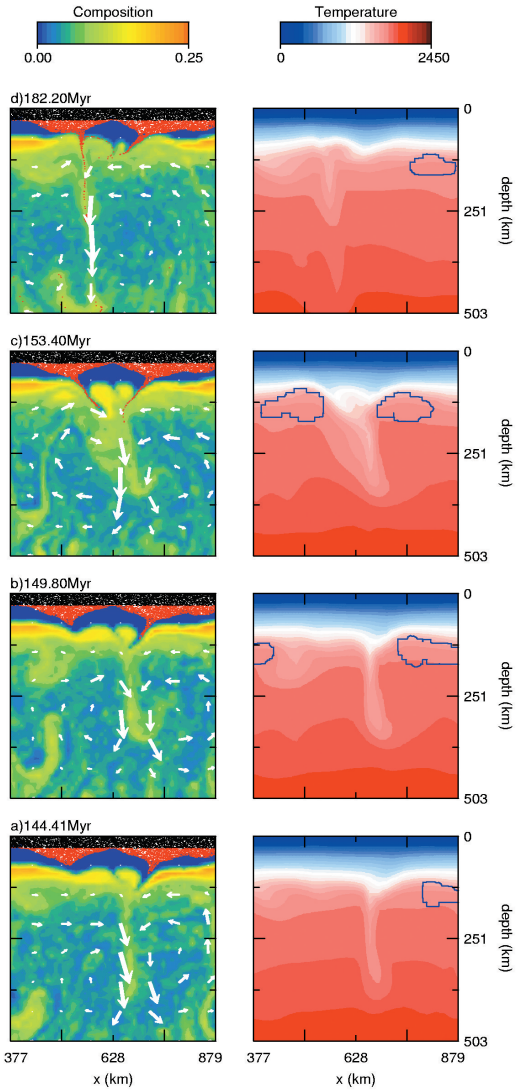

Figure 6.3: Four snapshots of composition and temperature from model Mr show how small scale circulations near the base of the crust allow recycling of eclogite into the mantle and production of new crust by partial melting of upwelling mantle peridotite. In the left hand side panels, the color scale from blue to orange indicates the degree of depletion F. Black and red tracers represent basalt end eclogite, respectively. The right hand side panels show the temperature field (color scale in degrees Celsius) and areas were partial melting is taking place (inside the contours).

diapiric ascent is stopped by the rapid increase of the temperature dependent viscosity (Figure 6.4b, note that the identical times of snapshots a and b indicate extremely fast upwelling in less than 10 kyr). The diapir head spreads out and the left-hand side rises further (Figure 6.4c) and melts up to a degree of nearly 0.30. The original diapir spreads out over nearly the entire domain of 1005 km. The large volume of melt produced locally thickens the crust by over 40 km (Figure 6.4d). The timescale on which this event takes place is extremely short. Although inflow of lower mantle material and partial melting continue for some millions of years, the rise of the diapir head through the upper mantle takes place in less than 20 kyr. This is the effect of the non-linear component of the rheology, as has been shown in the literature (Weinberg and Podladchikov, 1994; Larsen et al., 1997; Larsen and Yuen, 1997; Van Keken, 1997; Van Thienen et al., 2003a, chapter 8).

At least as catastrophic is the third type of dynamics, which is characterized by large scale delamination of a thickened crust into the mantle. Figure 6.5 shows the entire domain, starting just after the diapir event shown in Figure 6.4. The deeper part of the crust that is significantly thickened turns into eclogite in about 2 million years (Figure 6.5a) and sinks into the mantle. The right-hand side frame of Figure 6.5a shows that partial melting is taking place in the zone where material is sucked into the zone of upwelling created by the sinking crustal block. As the crustal block is quite cold and strong, it pulls down with it all the existing crustal material, which is mostly in the basalt phase and positively buoyant, see Figure 6.5b. Melting continues in the upper mantle, creating a new basaltic crust (Figure 6.5c). Note that this crust is significantly thinner (about 30 km) than the crust shown in Figure 6.5b. After the downgoing crust is sufficiently thinned it breaks off and further 'subduction' is halted. The basalt that was pulled down into the mantle has completely transformed into eclogite by now and the entire 'crustal lobe' sinks into the deeper mantle (Figure 6.5d). The complete replacement of the old crust by a new crust is illustrated by Figure 6.6, showing the variations of the formation age of crustal material. The figure, corresponding to the snapshot shown in Figure 6.5d, shows the old crust (blue) as it is sinking into the mantle, and the freshly produced crust (green, yellow, orange, purple) forming the new top of the domain. Note that the old crust has pulled down a significant amount of young crust (purple). In the upper part of the lower mantle, the subducted crust slowly heats up and becomes weaker. It breaks up allowing lower mantle peridotite to break into the upper mantle, while sinking crust replaces this material in the lower mantle (Figure 6.5d). Note the very short timescale of the whole process, where the replacement of the entire shallow crust takes place in less than 2 million years. The settling of the crust into the lower mantle to the bottom of the model domain takes much longer, on the order of 300 million years as both the density contrast between the sinking crust and the mantle decrease and the viscosity increases with depth (and decreasing strain rate).

6.3.3 Long-term thermal and chemical development

The thermal evolution of model Mr is illustrated in the lower panel of Figure 6.7 by the blue curve, showing the volume averaged temperature as a function of time. Three stages

can be discerned. During the first stage, lasting about 230 Myr, small scale delamination and crustal growth (see Figure 6.3) generate significant cooling of at a rate of about 300 K/Gyr (and crustal growth, as shown in the upper panel of Figure 6.7). The second, quite short, stage is characterized by rapid crustal growth and associated cooling, caused by lower mantle diapir ascent and complete resurfacing as shown in Figures 6.4 and 6.5. A drop in the volume averaged temperature of about 200^oC can be observed, and an average (over the entire domain width) of over 40 km of crust is produced . The third stage shows an absence of crustal growth, and because of this and the fact that the lower mantle temperature results in a thicker lithosphere, the cooling rate is reduced relative to the first two stages. No absolute numbers for cooling rates are given here since the small model domain (1005 km depth) does not allow comparison to the Earth, as will be discussed below (see section 6.3.4, where the larger model domain width and depth model Ms will be discussed).

The evolution of the incompatible trace element distribution of model Mr is illustrated in Figure 6.8, which shows the incompatible trace element concentration at different times during its evolution. The initial concentration of the trace element is 1, and the distribution coefficient is 10^{-2}. The ten frames in this figure show the concentration field at 10 subsequent times during the evolution of the model. Initially, the lower mantle is pristine. The upper mantle shows an increasing trace element depletion for shallower depths, where the mantle peridotite is subject to melting. This shallow partial melting also produces the enriched basaltic layer at the top boundary. After some 15 million years, slightly depleted upper mantle material is entrained into the lower mantle flow. As the recycling of eclogite into the mantle progresses, we see an increasing amount of grey colored enriched eclogite 'blobs' in the upper mantle (frames at 154.6 Myr and 228.9 Myr). The progressive cooling and the accumulation of eclogite blobs in the deepest upper mantle forces a breakdown of completely separate lower mantle and upper mantle convection (frames at 230.4-241.91 Myr), as predicted by Christensen and Yuen (1985). This brings more highly depleted material and enriched eclogite blobs into the lower mantle. Over the following 300 million years, the enriched crust sinks deeper into the lower mantle and settles at the bottom boundary. The upper and lower mantle continue to mix and form a more or less uniform reservoir of moderately depleted peridotite in which blobs of eclogite are dispersed. The high content of heat producing elements of the settled crust in the lower mantle makes it a heat source for convection in the mantle above, which may entrain some material from this layer. But essentially it remains stable for the remaining 500 million years of the model run.

The development of the bulk and incompatible trace element chemistry of this model (Mr) is presented in Figure 6.9. Time series of the averaged degree of depletion of the peridotite present are shown in Figure 6.9a for the entire domain, and for the lithosphere (0-150 km depth), the upper mantle (150-670 km depth) and the lower mantle (670-1005 km depth) separately. During the first 230 million years, we see a steady increase in the average degree of depletion of the entire domain of model Mr (Figure 6.9a). The lower mantle stays nearly pristine during this entire period. The upper mantle doubles its average degree of depletion over this period of time. However, as the interaction between the upper and lower mantle increases due to the cooling of the model and the

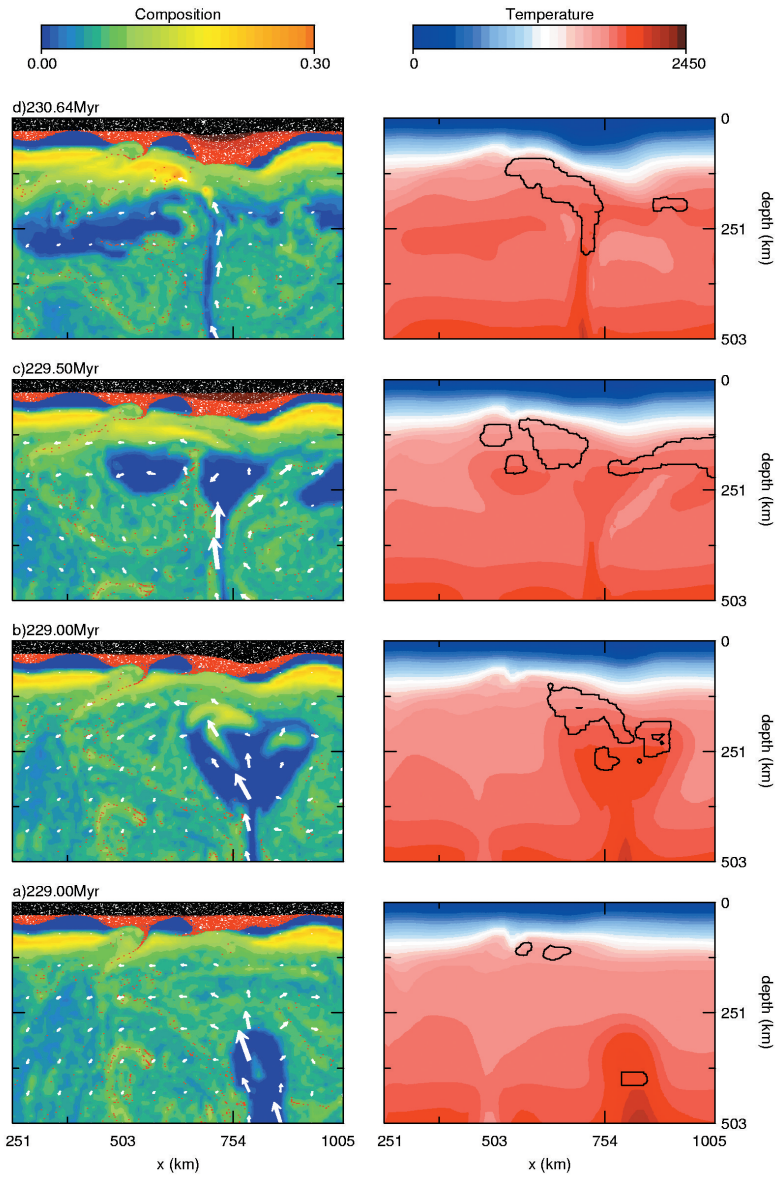

Figure 6.4: Four snapshots of composition and temperature from model Mr show the ascent and decompression melting of a mantle diapir, originating from the lower mantle. For an explanation of the colors, see the caption of Figure 6.3.

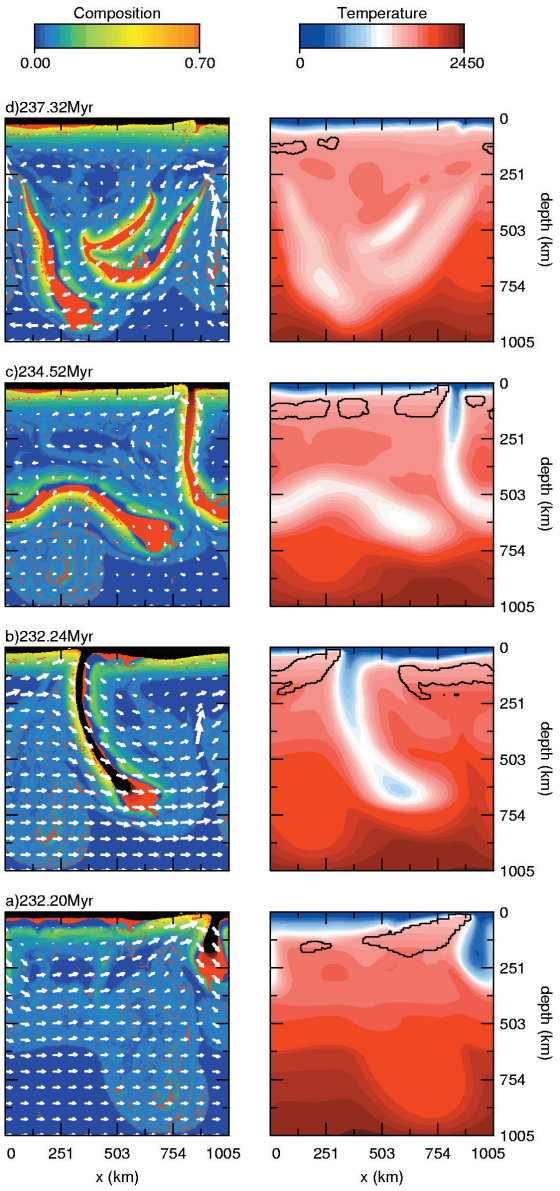

Figure 6.5: Four snapshots of composition and temperature from model Mr show the sinking of the entire crust into the mantle, driven by a large mass of dense eclogite. For an explanation of the colors, see the caption of Figure 6.3.

accumulation of eclogite blobs at the bottom of the upper mantle, some of the depleted material of the upper mantle is dumped into the lower mantle. The lithospheric degree of depletion fluctuates but shows a general decrease because more material is mixed into the upper mantle. After this initial stage, two important events (intrusion of a lower mantle diapir into the upper mantle and subsequent recycling of the thickened crust into the mantle) cause a marked increase in the averaged degree of depletion of the domain. The increase is observable in every reservoir, and practically at the same time (230 Myr). After this, the slow sinking of the crust and associated depleted mantle from the upper into the lower mantle causes an increase in the lower mantle value and a simultaneous decrease in the upper mantle value. Continued exchange of material between the upper and lower mantle reduces the difference over the following hundreds of million years, in line with the effective mixing illustrated in Figure 6.8.

Figure 6.9b shows the development of the approximate volume averaged incompatible trace element concentrations in the lithosphere, upper mantle and lower mantle. The same distinction in two separate phases can be made as in Figure 6.9a. During the first 230 million years, a steady increase in the average incompatible isotope concentration can be observed in the lithosphere. This is due to the accumulation of crust with a high concentration of the incompatible element. Complementary to this trend (but less pronounced because the reservoir is larger), we see a decrease in the average incompatible element concentration of the upper mantle, since the depleted residue that is formed upon partial melting is recycled through the upper mantle. The lower mantle shows a slight decrease in the concentration, which is due to radioactive decay. In the other curves, this is also present but invisible due to the larger effect of differentiation.

The two large scale events around 230 Myr (lower mantle diapir and large scale sinking of the crust into the mantle) have a strong impact on the average incompatible trace element distribution. As the crust forms an important reservoir for this element, its sinking into the lower mantle causes a strong decrease in the average trace element concentration in the lithospheric zone. Two causes can be named. Firstly, the new crust that is formed is much less volumous than the old crust which has been subducted. And secondly, the new crust was formed from already depleted mantle, so it will have lower average incompatible trace element concentrations. After these events, some entrainment of eclogite tracers from the settled crust at the bottom boundary of the model into the upper mantle somewhat increases the upper mantle average concentration and decreases it in the lower mantle. The effect of radioactive decay is visible in each curve.

6.3.4 Lower mantle size

As has been noted before, the lower mantle in our models is significantly smaller than in the Earth. Including a larger lower mantle at the same resolution, however, is computationally quite expensive. The size of the lower mantle is important for a number of reasons. It is a reservoir for both heat and undepleted peridotite. The models as presented in the previous sections are therefore capable of producing less crust than the Earth and they show a more rapid cooling than expected for the Earth.

Another important aspect is the layering of mantel convection. Christensen and Yuen

(1985) showed that the layering of mantle convection is a function of the Rayleigh number (see Table 6.1 for symbol definitions):

$$Ra = \frac{\rho_0 g \alpha \Delta T h^3}{\eta_0 \kappa} \tag{6.9}$$

In general, high Rayleigh number systems tend to develop a layered convection pattern in the presence of an endothermic phase boundary, whereas low Rayleigh number systems would tend to a whole mantle convection pattern. This suggests that the breakdown of layered convection as takes place e.g. model Mr around 230 Myr (see Figures 6.4 and 6.5) would be delayed in a system with a higher Rayleigh number. In order to test the sensitivity of the results to the depth of the lower mantle part of the model, we have done experiments with an increased domain width (and depth) of 1200 km (model Ms, see Table 6.2), resulting in a lower mantle depth of 530 km. The resulting dynamics of the extended model described above are summarized in the time series of volume averaged temperature and total amount of crust produced in Figure 6.7. Curves for the base model Mr can be used for comparison. As is illustrated by both strong drops in temperature and strong increases in the amount of crust produced, model Ms has a similar resurfacing event as described in section 6.3.2 and shown in Figure 6.5 for model Mr. The model shows a higher melt productivity than the smaller model Mr at a comparable cooling rate. This is a direct result of the reduced surface to volume ratio. Furthermore, the higher volume of fertile peridotite that can act as a source rock for basaltic material allows more crust to be produced. The extended model Ms also shows continued melting (although at a low rate) after the resurfacing event, in contrast to the behavior of model Mr, which shows no more melting after resurfacing.

Although because of the higher Rayleigh number of model Ms, it would be expected that layered convection is maintained for a longer period of time in this models than in model Mr (only 1005 km depth), the extended model shows a somewhat higher crustal production rate and generates a thick unstable crust on a shorter time scale, which causes resurfacing on a shorter time scale as well. Clearly the fact that we are dealing with thermo-chemical convection rather than merely thermal convection frustrates predictions based on the results of Christensen and Yuen (1985) and Steinbach and Yuen (1993) who find stronger layered convection for higher Rayleigh numbers. For the Earth, episodic switching between whole mantle convection and layered mantle convection has been inferred from geochemistry (Stein and Hofmann, 1994) and modeled by Breuer and Spohn (1995). In the extended model Ms, partially layered convection does take place after the resurfacing events, but a complete separation of upper and lower mantle is no longer observed.

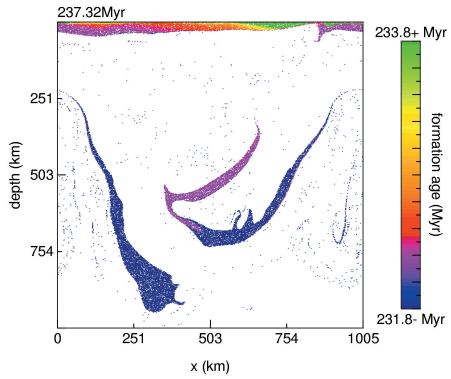

Figure 6.6: The formation age of every basaltic/eclogitic tracer in the domain of model Mr at 237.32 Myr is shown in color. Tracer ages outside the color scale are dark blue (older) or green (younger). The complete domain of 1005x1005 km is shown.

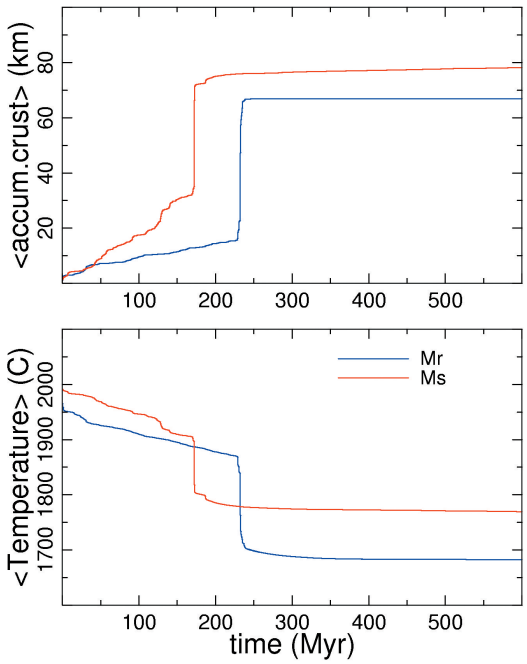

Figure 6.7: Time series of volume averaged temperature (bottom panel) and accumulated amount of created crust represented as an average thickness over the entire domain with (top panel), for models Mr and Ms (larger domain of 1200 km depth).

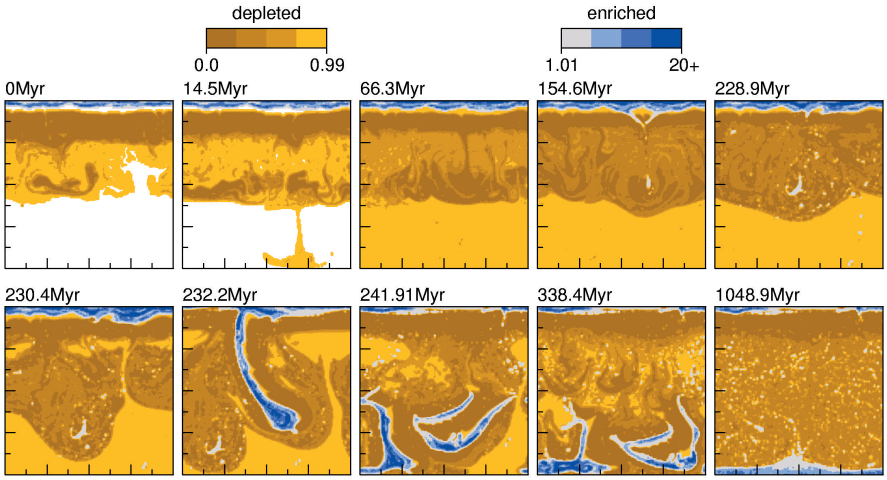

Figure 6.8: Ten snapshots of the trace element concentration field illustrate the chemical differentiation of model Mr. Pristine, undifferentiated material is white. Material that is depleted in trace elements is yellow, and the enriched melt products are blue. The distribution coefficient applied is 10^{-2}.

6.4 Discussion

6.4.1 Large Archean mantle plumes

The strong temperature dependence of the viscosity of the mantle causes the maximum horizontal temperature variations that can be created in the convecting mantle to be a function of mantle temperature (McKenzie and Bickle, 1988). For the present mantle, plume excess temperatures are estimated to be up to 200 to 250 Kelvin (Herzberg and O'Hara, 1998). In a hotter Archean mantle, this would be reduced to about 50 to 150 Kelvin (Nisbet et al., 1993). However, the mantle diapir that enters the upper mantle in model Mr (Figure 6.4) shows excessive melting due to its high excess temperature of about 250 Kelvin. Clearly the argument of reduced maximum excess temperatures for plumes in a hotter mantle of McKenzie and Bickle (1988) and Nisbet et al. (1993) breaks down for plumes originating from a breakthrough between layered convection cells as illustrated here. This demonstrates that in a hotter mantle, which will show a stronger layering of mantle convection (Christensen and Yuen, 1985), plumes with high excess temperatures and massive melting are feasible.

6.4.2 Rapid resurfacing

In section 6.3.2 we have seen that the entire crust may periodically sink into the mantle (see Figure 6.5). In the case of such an event, it is completely replaced by new crust, and a large amount of heat is released from the mantle. The crust sinks because of gravitational instability, caused by the transformation of basalt into eclogite in a crust significantly thickened by the breakthrough of lower mantle material into the upper mantle. An important parameter is the rheology of the sinking crust. In Figure 6.5 it is strong enough to pull down the entire existing (and partly positively buoyant) crust, such that a strong downward force localized at the site of the thickened crust causes resurfacing of the entire model. This type of dynamics resembles models for the dynamics of Venus during its history. Crater counts on the surface of Venus indicate that this planet underwent a global resurfacing event about 500 million years ago (Schaber et al., 1992). Different mechanisms have been proposed to explain the resurfacing event(s). Herrick and Parmentier (1994) suggest on the basis of thermal evolution calculations that the episodic reversal of two layers in the mantle may trigger a period of massive volcanism that completely renews the crust. Solomatov and Moresi (1996) suggest that plate tectonics was active on Venus before 500 Ma, which stopped because the stresses in the lithosphere dropped below the yield strength. A similar argument is used by Fowler and O'Brien (1996) to explain episodic heating of the mantle under a thickening stagnant lid, which experiences increasing buoyancy induced stresses during its cooling up to the point where plastic failure occurs and the lithosphere can subduct into the mantle. Turcotte (1995) compares 'episodic subduction' (p. 16,935) on Venus to the foundering of the solidified crust on a cooling lava lake. Due to the cooling of the crust, it becomes gravitationally unstable and sinks into the lake in parts that are separated by cracks. Our results most resemble the model of Parmentier and Hess (1992), in which the lithosphere episodically becomes negatively buoyant due to cooling, causing it to sink into the mantle. Secondly the basalt to eclogite phase transition in the lower crust causes parts of it to become negatively buoyant and recycle into the mantle. The material sinking into the mantle makes room for new partial melting of mantle peridotite, generating new crustal material an a depleted root, which can start to cool again. The results of Parmentier and Hess (1992) indicate that this process could take place on Venus with a periodicity of 300 to 500 million years. No spatial scale of recycling of lithosphere into the mantle is included in their model. Our results show recycling of eclogite and also depleted peridotite into the mantle on two scales: small-scale delaminations and large-scale sinking of the entire lithosphere into the mantle. However, Parmentier and Hess (1992) assume that eclogite which sinks into the mantle completely mixes with it, also chemically, essentially refertilizing the mantle. The mechanism of mantle refertilization by reaction with eclogite (Yaxley and Green, 1998) is not included in our model. Furthermore, as our model domain includes only a small part of the lower mantle corresponding to the width of the domain, a reduced amount of fertile peridotite and heat is present in our models, which further limits the maximum amount of crust that may be produced.

6.4.3 Thermal evolution of the mantle

Although the limited size of the lower mantle in our models does not allow quantitative statements on the absolute cooling rate of the Earth, the results do show that specifically the resurfacing mechanism as illustrated in Figure 6.5 is a strong cooling agent. The volume averaged temperature curves of Figure 6.7 show temperature decrease values of about 100 to 200^oC for a single resurfacing event in each model. We speculate that such a mechanism may have caused rapid cooling in the early history of the Earth over a period of several hundreds of millions of years until the temperature dropped to levels where the mechanisms described in this work are no longer viable.

6.4.4 Geochemical evolution of the mantle

Geochemical studies indicate that the earliest rocks found on Earth were already derived from a depleted mantle (Hamilton et al., 1983; Patchett, 1983; Vervoort et al., 1996; Blichert-Toft et al., 1999). Based on Hf isotope data, this depleted mantle was derived from a uniform chondritic reservoir at least 4.08 billion years before present (Amelin et al., 2000). Furthermore, the compiled isotope data from different Archean terranes suggest that during the Archean the mantle source of greenstone belts became more depleted with time (Condie, 1990; Amelin et al., 2000). Our model results are consistent with this observation. Figure 6.9 shows a steady, though not constant, increase of the averaged extracted melt degree for the upper mantle during the first 230 million years of the model evolution for model Mr. The same trend is illustrated in the incompatible element concentration plots for this model in Figure 6.8, which shows increasingly darker colors (i.e. lower concentrations) in the model upper mantle during the first 230 million years. The small extent of this model lower mantle limits the amount of fertile mantle peridotite that may be transported into the upper mantle. Influx of fresh lower mantle material would lower the average degree of depletion in the upper mantle, as can be observed in Figure 6.9a between 230 and 300 million years.

The range in trace element compositions found in basalts from different geodynamical settings on the present-day Earth indicates that the mantle contains several more or less separate geochemical reservoirs (Hofmann, 1997). Tackley (2000) gives an overview of different models which have been suggested to explain the presence of these reservoirs in the mantle. Furthermore, trace element balance calculations require a 'hidden' reservoir of enriched material apart from the continental crust and the depleted mantle reservoirs to comply with the assumption of a chondritic bulk silicate Earth (e.g. Galer and Goldstein, 1991; McDonough and Sun, 1995). This is also supported by the observation of subchondritic ratios of Nb/La, Nb/Ta, and possibly Ti/Zr in continental crust, depleted mantle and mid-ocean ridge basalt (Rudnick et al., 2000). Rudnick et al. (2000) propose that the missing Nb, Ta and possibly Zr reside in a reservoir of eclogite that underwent partial melting during subduction. They calculate that this reservoir should have a mass of about 0.5 to 6 % of the silicate Earth to compensate for the deficit. The subduction and storage of eclogite in the lower mantle as a mechanism of creating an enriched reservoir in the lower mantle has been investigated in numerical convection models by Christensen

and Hofmann (1994). Our model results show that subduction in the plate tectonics sense is not required to bring large amounts of eclogite into the lower mantle, and keep it there.

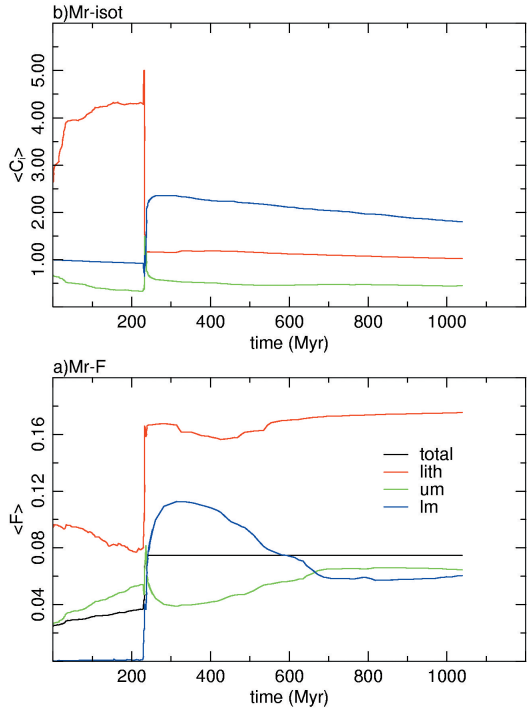

Figure 6.9: The chemical evolution of model Mr is presented in the form of time series for the averaged degree of depletion (a) and the averaged trace element concentration (b). Averaged values for the entire domain are shown in black. A subdivision has been made into the lithosphere (0-150 km depth, red curves), the upper mantle (150-670 km depth, green curves) and the lower mantle (670-1005 km depth, blue curves).

Though the small-scale delamination as described in section 6.3.2 and shown in Figure 6.3 only generates more or less uniformly distributed blobs of eclogite in the entire model mantle, large-scale crustal sinking as shown in Figure 6.5 does generate an enriched reservoir (see Figure 6.8) in the lower mantle which is stable for hundreds of millions of years at least. In recent years geodynamical models have been proposed featuring a dense enriched layer in the bottom third of the mantle (Coltice and Ricard, 1999; Kellogg et al., 1999; Van der Hilst and Kárason, 1999; Albarède and Van der Hilst, 2002), consisting of either primitive or recycled material. We speculate on the basis of our modelling results that such a layer may have been formed during a short time window in the early evolution

of the Earth's mantle by compositional differentiation in pressure release partial melting of mantle peridotite and subsequent large scale sinking of the thick basaltic/eclogitic crust into the lower mantle as an alternative to or precursor of the subduction model proposed by Albarède and Van der Hilst (2002). The resulting reservoir would distinguish from a primitive reservoir by its outgassed nature (low He content, developing a low ^{3}He/^{4}He ratio).

6.5 Conclusions

As argued in the introduction, the geodynamics of the early Earth was probably very different from the recent situation. Our model results, relevant for the hotter conditions in the early Earth, indicate that a number of processes may have been important:

- Small-scale ($x \cdot 10^2 km$) circulations of the shallow upper mantle and the lower crust, with partial melting in the upwelling limb of the convection and delamination and recycling of eclogitic lower crust in the downwelling limb, active over extended periods of time ($x \cdot 10^6 yr$).
- Episodic large-scale resurfacing events, in which a large part of or even the entire crust sinks into the mantle and is replaced by new crust at the surface. These events are quite rapid and take place within a few millions of years.
- Very fast penetration (5 m/yr) of lower mantle diapirs into the upper mantle, bringing hot and fertile mantle material to supersolidus conditions. This process generates large amounts of melt that may locally significantly thicken the crust ($x \cdot 10km$) and subsequently trigger the aforementioned process of resurfacing.

An important consequence of the latter process is that the penetration of lower mantle diapirs into the upper mantle in a layered convection system allows plume excess temperatures that are significantly higher (about 250 K) than the maximum plume excess temperatures which are predicted from the modified boundary layer theory of McKenzie and Bickle (1988) as applied to the Archean (about 50-150 K) by Nisbet et al. (1993). The episodic resurfacing in particular may have contributed to the formation of a bottom reservoir enriched in incompatible elements, as the 'subducted' crust sinks into the model lower mantle and forms a stable layer at the bottom boundary. We speculate that such a process may be responsible for the complete resurfacing of Venus which is dated at about 500 Ma from crater counts.